Rapid Communications

Skyrmion and tetarton lattices in twisted bilayer graphene

Thomas Bömerich, Lukas Heinen, and Achim Rosch*
Institute for Theoretical Physics, University of Cologne, D-50937 Cologne, Germany

(Received 5 May 2020; revised 25 August 2020; accepted 9 September 2020; published 21 September 2020)

Recent experiments on twisted bilayer graphene show an anomalous quantum Hall (AQH) effect at filling of three electrons per moiré unit cell. The AQH effect arises in an insulating state with both valley and ferromagnetic order. We argue that weak doping of such a system leads to the formation of a novel topological spin texture, a "double-tetarton lattice." The building block of this lattice, the "double-tetarton," is a spin configuration which covers 1/4 of the unit sphere twice. In contrast to skyrmion lattices, the net magnetization of this magnetic texture vanishes. Only at large magnetic fields are more conventional skyrmion lattices recovered. But even for large fields the addition of a single charge to the ferromagnetic AQH state flips hundreds of spins. Our analysis is based on the investigation of an effective nonlinear sigma model which includes the effects of long-ranged Coulomb interactions.

DOI: 10.1103/PhysRevB.102.100408

Twisted bilayer graphene (TBG) has emerged as a highly tunable platform to observe correlated electron behavior, such as insulating phases or unconventional superconductivity [1–3]. By twisting two sheets of graphene by an angle θ, a moiré pattern emerges and gives rise to a larger superlattice unit cell. The corresponding Brillouin zone (BZ) is much smaller than the BZ of a single graphene sheet and thus is called mini-BZ. At a "magic" twist angle of $\theta \approx 1.1^\circ$ the bands near the Fermi energy become exceptionally flat [4–8]. As the kinetic energy in these bands is small, electron-electron interactions become increasingly important. Because of spin and valley degeneracies the bands in the mini-BZ are fourfold degenerate. Besides controlling the band structure via the twist angle, the charge-carrier density in twisted bilayer graphene can also be controlled by external electrostatic gating.

In the beginning of 2019, Sharpe *et al.* found experimental evidence for a ferromagnetic state at filling $\nu = 3$ [9]. They measured an anomalous Hall effect which shows a hysteresis in an external magnetic field. There are many publications suggesting that the interactions may lift spin and valley degeneracies which could lead to different kinds of magnetic order [10–16]. Later in 2019, a quantized anomalous Hall effect was measured by Serlin *et al.* in TBG on a hexagonal boron nitride (h-BN) substrate for filling $\nu = 3$ [17]. Because of the substrate the twofold rotation symmetry of the TBG is broken, which gaps out the Dirac cones and the electronic bands aquire a nonzero Chern number C [18–22]. As the resulting ground state is a fully spin- and valley-polarized Chern insulator at filling $\nu = 3$ [15,23–26], there can be other charged excitations besides simple particle-hole pairs, namely, skyrmions.

In the quantum Hall phase there is a sizable Mott gap for charge excitations. Experimentally an activation gap of 30 K has been measured in transport [17,27]. Similarly, the valley degree of freedom is also gapped as its continuous rotation triggers a sign change of σ_{xy} and thus closes the charge gap. Therefore, we do not expect topological textures involving the valley degree of freedom [28] and focus our study on the only remaining low-energy degree of freedom, the magnetization. The spin structure can be described by a continuous vector field describing the classical magnetization $\hat{m}(\mathbf{r}, t)$. A skyrmion has a nontrivial topology characterized by its winding number W:

$$W = \frac{1}{4\pi} \int_{\mathbb{R}^2} d^2 r\, \hat{m}(\mathbf{r}) \cdot \left(\frac{\partial \hat{m}}{\partial x} \times \frac{\partial \hat{m}}{\partial y} \right) \in \mathbb{Z}. \tag{1}$$

If the Chern number of the electronic bands is independent of the spin orientation (as in the case of TBG), the skyrmion aquires a charge given by the product of Chern and winding number [29]. Skyrmions are fermionic (bosonic) for odd (even) products. Interestingly, it has been argued [30] that superconductivity can arise from the condensation of bosonic skyrmions for $C = 2$.

Long ago, it has been established both theoretically [31–33] and experimentally [34], that spin-polarized electrons in the Landau levels of quantum Hall systems can form skyrmions which carry electric charge. The same is true for flatbands with a finite Chern number. The electric charge density ρ_{el} in this case is proportional to the topological winding density ρ:

$$\rho_{\text{el}} = Ce\rho \quad \text{with} \quad \rho = \frac{1}{4\pi}\, \hat{m} \cdot \left(\frac{\partial \hat{m}}{\partial x} \times \frac{\partial \hat{m}}{\partial y} \right). \tag{2}$$

In the following we will numerically investigate topological textures induced by gating. Besides the expected skyrmion lattices we also find novel textures, which we dub double-tetarton lattices. We study the phase diagram in a magnetic field and argue that a rapid change of magnetization as a function of doping is a smoking gun signature of the double-tetarton phase.

*rosch@thp.uni-koeln.de

 ©2020 American Physical Society

The model. The free energy of the magnetic sector can be described by a nonlinear sigma model [31]:

$$F[\hat{m}] = \frac{J}{2}\int_{\mathbb{R}^2}(\nabla\hat{m})^2 d^2\mathbf{r} - \int_{\mathbb{R}^2}\mathbf{B}\cdot\hat{m}\,d^2\mathbf{r} + \frac{U_c}{2}\int_{\mathbb{R}^2}\int_{\mathbb{R}^2}\frac{[\rho(\mathbf{r})-\Delta\nu][\rho(\mathbf{r}')-\Delta\nu]}{|\mathbf{r}-\mathbf{r}'|}d^2\mathbf{r}\,d^2\mathbf{r}'. \tag{3}$$

Here all lengths are measured in units of $L_M = \sqrt{A_M} \approx 12\,\text{nm}$, where A_M is the area of the moiré unit cell [1]. The first two terms describe the spin stiffness J of the ferromagnetic state and a Zeeman coupling to an external field B. The third term is the long-ranged Coulomb interaction, $U_c = \frac{C^2e^2}{4\pi\epsilon_0\epsilon L_M}$, between (topological) charges, where ρ is the topological charge density defined in Eq. (2). J, B, U_c have units of energy. $\Delta\nu$ is a background charge measured from filling $\nu = 3$, which can be controlled by an external gate. We assume that the distance to the gate is much larger than the average distance of charges. In this limit, the average charge density is fixed by $\Delta\nu$:

$$\int_{\mathbb{R}^2}[\rho(r)-\Delta\nu]d^2r = 0. \tag{4}$$

A scaling analysis, where all lengths are rescaled by the factor λ, reveals that the Coulomb energy and Zeeman energy scale with λ^{-1} and λ^2, respectively, while the exchange term remains invariant. Coulomb repulsion (Zeeman energy) favors large (small) skyrmions. By minimizing the energy with respect to λ, one obtains an estimate for the radius of a single skyrmion in a magnetic field

$$R \sim L_M\left(\frac{U_c}{B}\right)^{1/3} = R^*. \tag{5}$$

Ground state for $B = 0$. To determine the ground state in the absence of a magnetic field at fixed winding number density, we performed numerical simulations for different unit-cell geometries (see Supplemental Material [35]). The lowest energy is found for a triangular lattice with a hexagonal unit cell shown in Fig. 1. We first note that the total winding number within the magnetic unit cell (white hexagon in Fig. 1) is -2, but the resulting spin configuration is *not* a lattice of skyrmions. The primary building block is instead the magnetic structure in the central black hexagon of Fig. 1. Here the spins cover exactly one-quarter of the unit sphere *twice* (a skyrmion covers the full unit sphere once). When one tracks the direction of spins moving along the edge of the central black hexagon, one obtains a path shown in Fig. 2 which winds twice around the north pole. In analogy to a "meron" (half of a skyrmion), we call this structure "double-tetarton."

Moving from one black hexagon to the six next-nearest neighbors, the magnetic structure is rotated by 180° around one of the three axes shown in Fig. 2. The group of magnetic symmetry transformations is—up to the translations—isomorphic to the octahedral group O_h (see Supplemental Material [35]). Four double-tetartons thereby give the magnetic unit cell which therefore has winding number $W = 4\times 2\times(-\frac{1}{4}) = -2$. By symmetry, the ground state has no net magnetization $\int m_i(\mathbf{r})d^2r = 0$. This is an important observation which distinguishes our double-tetarton lattice from skyrmion lattices. Furthermore, we can look at the contours of the electric charge density depicted in Fig. 1. The black hexagons define the unit cell of the charge density which has minima in their centers. The spin configuration spontaneously breaks global spin-rotation invariance and one can thus obtain other configurations just by rotating all spins (see Supplemental Material [35]); the charge density remains invariant under such rotations. In the limit $U_c \to 0$, when the energy is only determined by the exchange interaction, the energy E_{UC} per magnetic unit cell of the double-tetarton lattice is in the continuum limit exactly given by $E_{\text{UC}} = 8\pi J$, twice the energy of the Polyakov skyrmion [36]. This follows from the fact that the Polyakov skyrmion is a lower bound for the energy per winding number of topological textures in the presence of exchange interactions and that one can also construct an upper bound to the energy using lattices of Polyakov skyrmions.

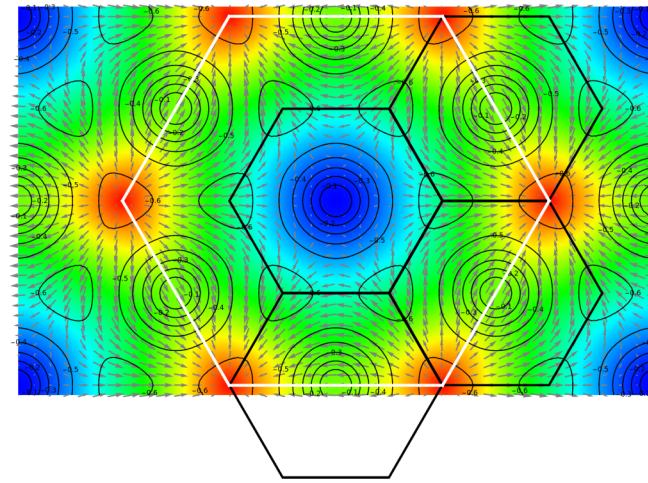

FIG. 1. Ground-state spin configuration for $B = 0$ and $\Delta\nu(\frac{U_c}{J})^2 = 0.098$ (gray arrows: magnetization in the x-y plane; colors: z component of the spin with blue for up and red for down spins). The total winding number within the magnetic unit cell (white hexagon) is $W = -2$. The black hexagons depict the building blocks of the magnetic structure, a "double-tetarton" (see text and Fig. 2). The figure also shows contour lines of the topological charge density.

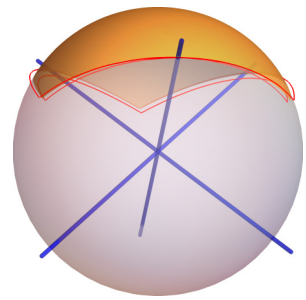

FIG. 2. The basic building block of the texture shown in Fig. 1 is a "double tetarton": the spins cover exactly one-quarter of the unit sphere twice. The red line shows a path along the edge of the central black hexagon which winds twice around the colored area. The magnetic texture of the other hexagons in Fig. 1 can be obtained by rotating the spins by 180° around one of the blue axes.

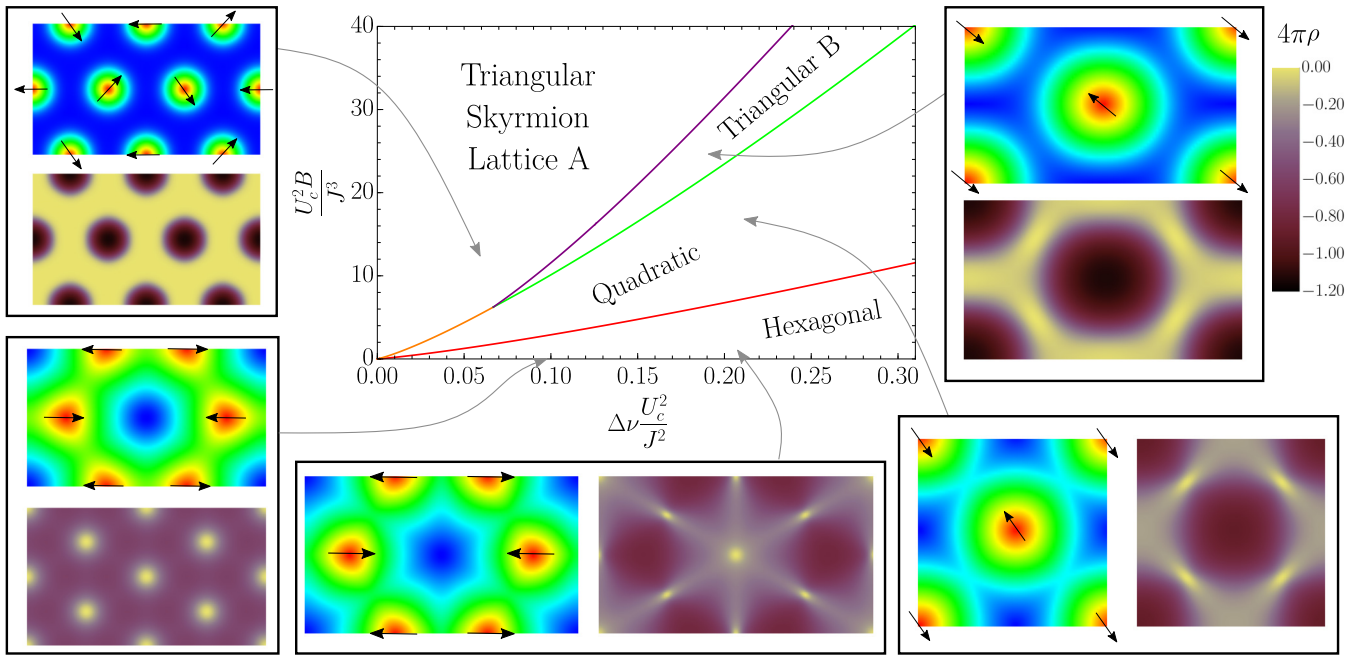

FIG. 3. Phase diagram for magnetic textures with Coulomb interactions. One representative spin configuration (color scale as in Fig. 1; arrows indicate the helicity) and the corresponding charge density for each phase is shown. In the case of $B = 0$ the double-tetarton lattice (lower left corner) is the ground state. For small magnetic fields a hexagonal lattice has the lowest energy (lower middle picture), while at low density and large magnetic field the ground state is a triangular lattice of skyrmions with 120° helicity order (upper left corner). At intermediate fields we obtain a triangular lattice with striped helicity order as well as a square lattice with an "antiferromagnetic" helicity order.

It is also consistent with our numerical results where we obtain for small U_c, $E_{UC} \approx 8\pi J + 0.04 U_c \sqrt{\Delta\nu}$. If this energy is smaller than twice the Mott gap (the energy required to add two electrons into higher bands), then a topological magnetic texture will form whenever the system is doped slightly.

Phase diagram. In Fig. 3 the phase diagram as a function of doping and magnetic field is shown. A small magnetic field in the z direction breaks the $O(3)$ spin-rotation invariance. Numerically we find (see Supplemental Material [35]) that for a small magnetic field in the z direction, the ground state smoothly evolves from the double-tetarton configuration shown in Fig. 1. Due to the lowered symmetry, the double-tetarton lattice can now be smoothly deformed to a hexagonal lattice of skyrmions located at the six edges of the magnetic unit cell. Each skyrmion has an internal degree of freedom, called "helicity," which can be identified with the in-plane spin direction when moving from the skyrmion center in the $+\hat{x}$ direction. In the hexagonal small-field phase, the helicity (arrows in Fig. 3) shows an antiferromagnetic order.

In the opposite limit of large magnetic fields and small densities, the ground state is given by magnetic skyrmions in a ferromagnetic background. These skyrmions are small and far apart from each other, so we can treat them as pointlike particles which interact via Coulomb interactions. To minimize Coulomb repulsions, they form a triangular lattice. For large skyrmion distance, the helicity forms a 120° order (triangular phase A), reminiscent of the magnetic order of antiferromagnetically coupled spins on triangular lattices. Indeed the helicities of neighboring skyrmions are weakly (exponentially suppressed in the skyrmion distance) antiferromagnetically coupled via the ferromagnetic exchange interaction of spins. When the skyrmion radius $R \sim (U_c/B)^{1/3}$ becomes of the same order as the skyrmion distance $\sim 1/\sqrt{\Delta\nu}$, i.e., for $B \sim U_c(\Delta\nu)^{3/2}$, the skyrmions deform and helicity order changes to a striped state with opposite helicities (triangular phase B). Furthermore, we also obtain a centered square lattice between the hexagonal phase and the triangular skyrmion phases (see Fig. 1). In this phase the skyrmions show antiferromagnetic helicity order.

For an order-of-magnitude estimate of experimental parameters we assume $J \sim 10\,\text{meV}$ (of the same order of magnitude as the bandwidth) and $U_c = \frac{e^2}{4\pi\epsilon\epsilon_0 L_M} \sim 100\,\text{meV}$ (assuming $\epsilon \sim 1$). In our units a magnetic field of 1 T is equivalent to $B = 0.06\,\text{meV}$. The triple point in the phase diagram Fig. 3, where the triangular and the quadratic phases meet, is therefore predicted to occur at a doping of $\Delta\nu \approx 0.066(J/U_c)^2 \sim 10^{-3}$ and a field of $B \approx 6.3\frac{J^3}{\mu_B U_c^2} \sim 10\,\text{T}$. For a larger doping of a few percent, we expect that the system remains in the hexagonal phase for all experimentally accessible fields.

Magnetization. A central experimental signature [34] is the dependence of the magnetization per spin, m_z, on the charge or, equivalently, the skyrmion density. For $B = 0$ the ground state with finite winding number has zero net magnetization as discussed above. This implies that at $T = 0$ and for $B \to 0$, the magnetization jumps from a fully polarized state, $m_z = 1$, to a state with zero magnetization for an arbitrarily small doping, $|\Delta\nu| > 0$. The inset of Fig. 4 shows that at finite B field this jump is broadened to a crossover. For small $\Delta\nu$ the magnetization per skyrmion is given by

$$M_{\text{sky}} \approx 28\left(\frac{U_c}{B}\right)^{2/3} \sim R^{*2} \quad \text{for} \quad \Delta\nu \to 0, \tag{6}$$

which diverges for $B \to 0$, consistent with Eq. (5).

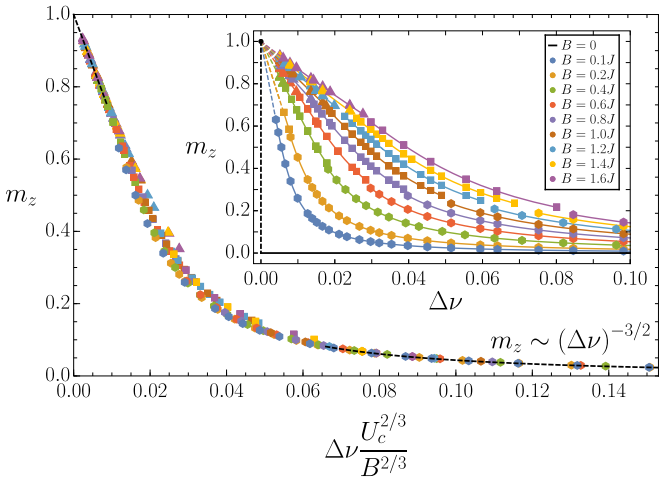

FIG. 4. Magnetization (in units of μ_B per TBG moiré unit cell) as a function of the (rescaled) charge density. Inset: For $B = 0$ the magnetization jumps to zero for infinitesimal doping. The jump is broadened at finite B. The shape of the markers (triangular, quadratic, or hexagonal) indicate the magnetic phases (triangular, quadratic, or hexagonal). Note that there are tiny jumps at the first-order transitions between two phases. Curves are taken for $U_c = 5J$.

This result suggests that the magnetization m_z is a function of $\Delta\nu(\frac{U_c}{B})^{2/3}$,

$$m_z \approx f\left[\Delta\nu\left(\frac{U_c}{B}\right)^{2/3}\right], \tag{7}$$

which is confirmed by the scaling plot of Fig. 4. Note that we obtain only tiny jumps in the magnetization when one crosses one of the first-order transitions of Fig. 3 and the magnetization of all phases is approximately described by the same scaling curve. For $B \to 0$, m_z is linear in B and therefore the scaling ansatz (7) predicts $f(x \to \infty) \sim x^{-3/2}$ or $m_z \sim (\Delta\nu)^{-3/2} B/U_c$ in this limit.

Our analysis has ignored the effects of dipolar interactions. Remarkably, simple power counting arguments show that dipolar interactions should become important in the limit of infinitesimal doping $\Delta\nu \to 0$. However, an analysis of the relevant prefactors shows that for realistic parameters the effects of dipolar interactions are negligible (see Supplemental Material [35]).

Discussion. Twisted bilayer graphene provides a unique opportunity to discover new topological states of matter. Importantly, the anomalous quantum Hall effect in this system observed for $\nu = 3$ is not induced by spin-orbit coupling but arises from the ordering of the valley degree of freedom. Thus the spin degree of freedom can rotate without closing the gap. We have argued that for small doping away from $\nu = 3$, one therefore naturally realizes a topological magnetic texture with finite winding number and zero net magnetization best described as a lattice of double tetartons, i.e., textures which cover $1/4$ of the unit sphere two times and which are connected to neighboring double tetartons by the three twofold rotation axes of a tetrahedron.

Experimentally, the most direct way to measure topological textures in twisted bilayer graphene is to use spin-polarized scanning tunneling microscopy. Also measurements of the magnetization as a function of the gate voltage can be used: whenever the number of flipped spins per added charge is large [according to Eq. (6) about 300 spins flip in a field of 10 T], this clearly indicates the presence of skyrmionic excitations. As the double-tetarton lattice carries zero magnetization, we predict that this number diverges in the low-temperature, low-field limit.

An interesting question is whether tetartons can exist as single particles. Here it is useful to consider the analogy with merons, half-skyrmions which cover $1/2$ of the unit sphere. They are realized in two-dimensional ferromagnets with an easy-plane anisotropy as vortex states [37,38]. Similarly, we have checked that tetartons covering exactly $1/4$ of the unit sphere naturally arise in two-dimensional ferromagnets with certain cubic anisotropies when, for example, three domains with orientation (1,1,1), $(1, -1, -1)$, and $(-1, 1, -1)$ meet. In (anomalous) quantum Hall systems with Chern number 1 such textures naturally carry the charge $1/4$.

For the future it will be interesting to investigate how such topological textures can be controlled by currents and fields and to explore possible classical and quantum liquids generated from such states.

Acknowledgments. The numerical simulations have been performed with the open-source micromagnetic simulation program MuMax3 [39,40] with custom additions [35] on the CHEOPS cluster at the RRZK Cologne. We thank S. Ilani, A. Vishvanath, and M. Zirnbauer for useful discussions and the Deutsche Forschungsgemeinschaft (DFG, German Research Foundation) for financial support (CRC1238, Project No. 277146847, subproject C02). We thank M. Antonoyiannakis and A. Melikyan for suggesting the name tetarton.

[1] Y. Cao, V. Fatemi, S. Fang, K. Watanabe, T. Taniguchi, E. Kaxiras, and P. Jarillo-Herrero, Nature (London) **556**, 43 (2018).

[2] Y. Cao, V. Fatemi, A. Demir, S. Fang, S. L. Tomarken, J. Y. Luo, J. D. Sanchez-Yamagishi, K. Watanabe, T. Taniguchi, E. Kaxiras, R. C. Ashoori, and P. Jarillo-Herrero, Nature (London) **556**, 80 (2018).

[3] M. Yankowitz, S. Chen, H. Polshyn, Y. Zhang, K. Watanabe, T. Taniguchi, D. Graf, A. F. Young, and C. R. Dean, Science **363**, 1059 (2019).

[4] E. Suárez Morell, J. D. Correa, P. Vargas, M. Pacheco, and Z. Barticevic, Phys. Rev. B **82**, 121407(R) (2010).

[5] J. M. B. Lopes dos Santos, N. M. R. Peres, and A. H. Castro Neto, Phys. Rev. Lett. **99**, 256802 (2007).

[6] J. M. B. Lopes dos Santos, N. M. R. Peres, and A. H. Castro Neto, Phys. Rev. B **86**, 155449 (2012).

[7] P. Moon and M. Koshino, Phys. Rev. B **85**, 195458 (2012).

[8] R. Bistritzer and A. H. MacDonald, Proc. Natl. Acad. Sci. USA **108**, 12233 (2011).

[9] A. L. Sharpe, E. J. Fox, A. W. Barnard, J. Finney, K. Watanabe, T. Taniguchi, M. A. Kastner, and D. Goldhaber-Gordon, Science **365**, 605 (2019).
[10] M. Xie and A. H. MacDonald, Phys. Rev. Lett. **124**, 097601 (2020).
[11] J. F. Dodaro, S. A. Kivelson, Y. Schattner, X. Q. Sun, and C. Wang, Phys. Rev. B **98**, 075154 (2018).
[12] A. Thomson, S. Chatterjee, S. Sachdev, and M. S. Scheurer, Phys. Rev. B **98**, 075109 (2018).
[13] M. Ochi, M. Koshino, and K. Kuroki, Phys. Rev. B **98**, 081102(R) (2018).
[14] N. Bultinck, E. Khalaf, S. Liu, S. Chatterjee, A. Vishwanath, and M. P. Zaletel, Phys. Rev. X **10**, 031034 (2020).
[15] S. Chatterjee, N. Bultinck, and M. P. Zaletel, Phys. Rev. B **101**, 165141 (2020).
[16] L. Klebl and C. Honerkamp, Phys. Rev. B **100**, 155145 (2019).
[17] M. Serlin, C. L. Tschirhart, H. Polshyn, Y. Zhang, J. Zhu, K. Watanabe, T. Taniguchi, L. Balents, and A. F. Young, Science **367**, 900 (2020).
[18] H. Kim, N. Leconte, B. L. Chittari, K. Watanabe, T. Taniguchi, A. H. MacDonald, J. Jung, and S. Jung, Nano Lett. **18**, 7732 (2018).
[19] J. Jung, A. M. DaSilva, A. H. MacDonald, and S. Adam, Nat. Commun. **6**, 6308 (2015).
[20] N. Bultinck, S. Chatterjee, and M. P. Zaletel, Phys. Rev. Lett. **124**, 166601 (2020).
[21] Y.-H. Zhang, D. Mao, Y. Cao, P. Jarillo-Herrero, and T. Senthil, Phys. Rev. B **99**, 075127 (2019).
[22] Y.-H. Zhang, D. Mao, and T. Senthil, Phys. Rev. Research **1**, 033126 (2019).
[23] J. Liu and X. Dai, arXiv:1911.03760.
[24] Y. Alavirad and J. D. Sau, arXiv:1907.13633.
[25] C. Repellin, Z. Dong, Y.-H. Zhang, and T. Senthil, Phys. Rev. Lett. **124**, 187601 (2020).
[26] F. Wu and S. Das Sarma, Phys. Rev. Lett. **124**, 046403 (2020).
[27] L. Balents, C. Dean, D. Efetov, and A. Young, Nat. Phys. **16**, 725 (2020).
[28] Y. Lian, A. Rosch, and M. O. Goerbig, Phys. Rev. Lett. **117**, 056806 (2016).
[29] F. Freimuth, R. Bamler, Y. Mokrousov, and A. Rosch, Phys. Rev. B **88**, 214409 (2013).
[30] E. Khalaf, S. Chatterjee, N. Bultinck, M. P. Zaletel, and A. Vishwanath, arXiv:2004.00638.
[31] S. L. Sondhi, A. Karlhede, S. A. Kivelson, and E. H. Rezayi, Phys. Rev. B **47**, 16419 (1993).
[32] H. A. Fertig, L. Brey, R. Côté, and A. H. MacDonald, Phys. Rev. B **50**, 11018 (1994).
[33] H. A. Fertig, L. Brey, R. Côté, A. H. MacDonald, A. Karlhede, and S. L. Sondhi, Phys. Rev. B **55**, 10671 (1997).
[34] S. E. Barrett, G. Dabbagh, L. N. Pfeiffer, K. W. West, and R. Tycko, Phys. Rev. Lett. **74**, 5112 (1995).
[35] See Supplemental Material at http://link.aps.org/supplemental/10.1103/PhysRevB.102.100408 for details on simulations, symmetry analysis, and influence of dipolar interactions.
[36] A. A. Belavin and A. M. Polyakov, Pisma Zh. Eksp. Teor. Fiz. **22**, 503 (1975) [JETP Lett. **22**, 245 (1975)].
[37] Y. A. Kharkov, O. P. Sushkov, and M. Mostovoy, Phys. Rev. Lett. **119**, 207201 (2017).
[38] S.-Z. Lin, A. Saxena, and C. D. Batista, Phys. Rev. B **91**, 224407 (2015).
[39] A. Vansteenkiste, J. Leliaert, M. Dvornik, M. Helsen, F. Garcia-Sanchez, and B. Van Waeyenberge, AIP Adv. **4**, 107133 (2014).
[40] L. Exl, S. Bance, F. Reichel, T. Schrefl, H. Peter Stimming, and N. J. Mauser, J. Appl. Phys. **115**, 17D118 (2014).